Asia-Pacific Journal of Atmospheric Sciences
https://doi.org/10.1007/s13143-021-00266-x

Online ISSN 1976-7951
Print ISSN 1976-7633

ORIGINAL ARTICLE

The Recent Abrupt Increase in South China Sea Winter Precipitation

JaeWon Choi[1] · Joong-Bae Ahn[2]

Received: 17 August 2021 / Revised: 10 November 2021 / Accepted: 30 November 2021

Abstract

The change of average winter precipitation in the South China Sea (SCS) since 1999 was investigated by analyzing the average precipitation between 1999 and 2014 and 1980–1993. The spatial distribution of the winter precipitation difference between the two periods showed that the negative anomalies were distributed from the equatorial eastern Pacific to the equatorial central Pacific, and the positive anomalies were distributed in the subtropical western Pacific, the Maritime Continent, and northern part of Australia, which is a typical spatial distribution of precipitation anomalies during La Niña events. In the tropical Pacific, the Walker circulation is intensified, in which air rises from the Maritime Continent and air in the tropical western Pacific descends at the equatorial central Pacific. Therefore, the change in sea surface temperature showed a typical La Niña pattern. In the East Asian regions, the local Hadley circulation in which air rises above the SCS and descends in the mid-latitudes of East Asia is intensified. This circulation is related to the anomalous pressure distribution of the west-high and east-low pattern in East Asia and the strengthening of the East Asian winter monsoon. In addition, this result is in-line with increased snow depth in mid-latitude East Asia in recent years.

Keywords Interdecadal variation · Winter precipitation · South China Sea · Walker and Hadley circulations

1 Introduction

Since the South China Sea (SCS) is located at the center of the Asian-Australian monsoon system and lies within the region where the East-Asian monsoon and the western North-Pacific monsoon are conjoined, the SCS summer monsoon (SCSSM) is one of the important elements of the Asian summer monsoon season (Murakami and Matsumoto 1994; Wang et al. 2009). The SCS located between the Western Pacific and the Indian Ocean is the largest coastal water in Southeast Asia. SCS has a basin structure with an average water depth of 1800 m and a maximum water depth of 5400 m (Twigt et al. 2007). The SCS is known to be influenced by the Southeast Asian monsoon and to produce various surface circulations in the regions surrounding southern China (Wyrtki 1961; Shaw and Chao 1994; Chu et al. 1999; Hu et al. 2000; Liu et al. 2001a, 2001b; Centurioni et al. 2009). During summer, the main wind direction is southwesterly in the SCS region, and a dominant clockwise surface circulation causes upwelling in the coastal areas of Vietnam, which maintains cold sea surface temperature (SST).

In particular, the net surface heat flux in the region is a major cause of SST variation (Liu et al. 2001b; Qu 2001), and shortwave radiation and latent heat have also been reported as major determinants of SST (Liu and Xie 1999; Wu 2002; Chen et al. 2003; Lestari et al. 2011). The SCS is part of the eastern Indian Ocean and western Pacific warm pools, where air-sea interactions are important (Wang et al. 1997; Wu and Wang 2001; Liu et al. 2004; Xie et al. 2007; Wu 2010). In particular, SSTs have shown a distinctive warming trend in recent years with interannual variations over the summer. This warming trend is believed to change the characteristics of air-sea interactions in this region. More specifically, an increase in the SST can cause surface evaporation and produce convergence of water vapor in the lower-level troposphere, generate convection in this region, and destabilize the atmosphere (Lestari et al. 2011). Thus,

Responsible Editor: Ashok Karumuri

✉ Joong-Bae Ahn
jbahn@pusan.ac.kr

[1] Institute for Basic Science, Pusan National University, Busan, South Korea

[2] Division of Earth Environmental System, Pusan National University, Geumjeong-gu, Busan 46241, Republic of Korea

Published online: 13 January 2022

an increase in SSTs in this region could be a major driver of convective activity and precipitation.

On the other hand, changes in atmospheric variables such as precipitation and cloud cover changes in this region affect other variables such as the amount of solar radiation reaching the sea, sea surface evaporation, and seawater mixing, resulting in changes in SST. Thus, changes in the characteristics of ocean and atmosphere in this region can lead to various climate variations through the interaction between ocean and atmosphere. In addition, these changes can affect the regional Hadley circulation in the south-north direction, resulting in weather and climate variations in the surrounding region of SCS. Accordingly, it is important to understand the changes in air-sea interaction characteristics in SCS in order to properly predict weather and climate in the surrounding region and East Asia as well as SCS (He and Wu 2012).

The SCSSM plays a critical role in determining the climate characteristics of the surrounding areas of SCS during the boreal summer (Ding 1992; Zhu et al. 2003). In addition, SCS is considered an important region in determining the variability of Asian monsoon because it is the first place where the summer monsoon develops in Asia (Lau et al. 2000). In particular, SST variations in SCS have been recently reported to the strongly influential in accordance with the characteristics of the East-Asian monsoon and global warming (Shin 2011). Therefore, studies on East Asia monsoon and the role of air-sea interactions in SCS are useful in identifying characteristics of East Asia summer climate system.

Interdecadal variation of the SCSSM has been the subject of much discussion in recent years. Wang et al. (2009) showed that summer and autumn precipitation increased in southern China and northern SCS but decreased in the central SCS from 1993. They also examined interdecadal changes in seasonality by using season-reliant empirical orthogonal function (SEOF) analysis. However, no detailed analysis on such decadal changes has been performed, and the mechanisms involved have not been fully elucidated. Furthermore, interdecadal changes around 1993/1994 were found to be the result of the spatiotemporal structure of intraseasonal variability (ISV) in the SCS during boreal summers (Kajikawa et al. 2009). Moreover, Kajikawa and Bin (2012) discovered a clear interdecadal variation in 1993/1994 during SCSSM onset. Actually, the recent climate shift around the late 1990s featured a La Niña-like SST change over the Pacific basin, which has been associated with a phase shift of the Interdecadal Pacific Oscillation (IPO) from a warm to a cool phase. In fact, the phase shift to be examined in this study are related to the internal variation of IPO. These major decadal and multidecadal time scale mode variabilities in the Pacific have been identified by observational and modeling studies (e.g., Power et al. 1999; Meehl and Hu 2006; Deser et al. 2010; Delworth and Mann 2000; Zhang and Delworth 2006, 2007) and they can influence global-scale climate phenomena, such as rainfall in East Asian (Si and Ding 2016) or drought in the southwestern United States (Meehl and Hu 2006).

A small number of studies have been conducted on interdecadal variations of winter precipitation in the SCS. Zhang et al. (2014) reported enhanced winter precipitation over Southeast China after the 1990s and suggested that this was induced by variability of the Arctic Oscillation. Choi et al. (2016) found a significant decrease in winter rainfall over Southern China around the late 1990s, which may also be related to a change in Hadley circulation. Olaguera et al. (2018) identified an interdecadal shift in the winter monsoon in the Philippines around 1992/1993 and pointed out that the shift was most remarkable during December. The distribution of winter to winter variance showed a similar pattern, with large amplitudes in the SCS suggesting a higher probability of rainfall extremes. In this paper, we focus on the interdecadal variability of SCS winter rainfall to identify relevant large-scale atmospheric and oceanic flow patterns and mechanisms.

In Section 2, we introduce the analytic methods and materials used, and in Section 3, the interdecadal variation of SCS winter precipitation is studied. In Section 4, the causes of interdecadal variations in SCS winter precipitation are verified by analyzing large-scale environments. Finally, section 5 provides a summary of our results.

2 Data and Methods

2.1 Data

In this study, geopotential height (gpm), zonal and meridional winds (ms^{-1}), air temperature (°C), precipitable water (kgm^{-2}), and specific humidity (gkg^{-1}) (at multiple levels) data were obtained from the National Center for Environmental Prediction/National Center for Atmospheric Research (NCEP/NCAR) reanalysis I from 1980 to 2014 (Kalnay et al. 1996; Kistler et al. 2001). Merged analysis of precipitation (CMAP) data was obtained from the Climate Prediction Center (CPC), and reconstructed monthly sea surface temperatures were obtained from The National Oceanic and Atmospheric Administration (NOAA) (NOAA Extended Reconstruction SST V4; Huang et al. 2014; Liu et al. 2014).

2.2 Methods

The Student's *t* test was used to determine the significance of differences between means (Wilks 1995). In this study, boreal winter was defined as the period from December to February. For example, the boreal winter in 1983 included the period from the 1st December 1982 to the 28th February

1983. Niño-3.4 indices were derived by the Climate Prediction Center (CPC) of NOAA (http://www.cpc.noaa.gov/products/analysis_monitoring/ensostuff/ensoyears.shtml), and East Asian winter monsoon (EAWM) indices were derived using the method devised by Sun and Sun (1995) and area-averaged 500 hPa geopotential height over the region 30°-45°N, 125°-145°E. In this study, the SCS region was defined as the area bounded by 10°-20°N and 110°-120°E, as shown in Fig. 1.

3 Analysis of the Time Series of SCS Winter Precipitation

Figure 2 shows the time-series of the SCS winter precipitation, which over the past 35 years showed a clear significant increasing trend at the 95% confidence level (dashed line in Fig. 2). As depicted in the figure, SCS winter precipitation over the past 35 years was divided into three periods: 1980–1993 (red line), 1994–1998 (blue line), and 1999–2014 (brown line). Average precipitations during these three periods were 1.3, 2.2, and 2.7 mm day^{-1}, respectively. Average precipitation during 1999–2014 was twice that during 1980–1993, and the difference in average precipitation was significant at the 95% confidence level.

To determine whether any significant climate regime shift existed in this time series, statistical change-point analysis was applied (bold line). Because this variable did not follow a Poisson distribution, we used a log-linear regression model, in which a step function is expressed as an independent variable, to detect climate regime shifts in the temperature and passage frequency series. If the estimated slope is at least twice as large as its standard error, one may reject the null hypothesis (i.e., that the slope is zero) at the 5% significance level. The details of this method are well described by Elsner et al. (2000), Chu (2002), and Ho et al. (2004). When statistical change-point analysis has been conducted, a t-value is produced for each year. An absolute large t-value means that a significant climate regime shift occurred in that year. In the current study, significant climate regime shifts occurred in 1994 and 1999.

Thus, this study aims to analyze the average differences between 1999 and 2014 and 1980–1993 to determine the cause of the recent increase in the SCS winter precipitation.

4 Differences between 1999 and 2014 and 1980–1993

4.1 Seasonal Variations of Precipitable Water

Figure 3a shows seasonal variations of precipitable water during 1994–2014 and 1980–1993. Precipitable water was greater during the winters and springs of 1994–2014 than

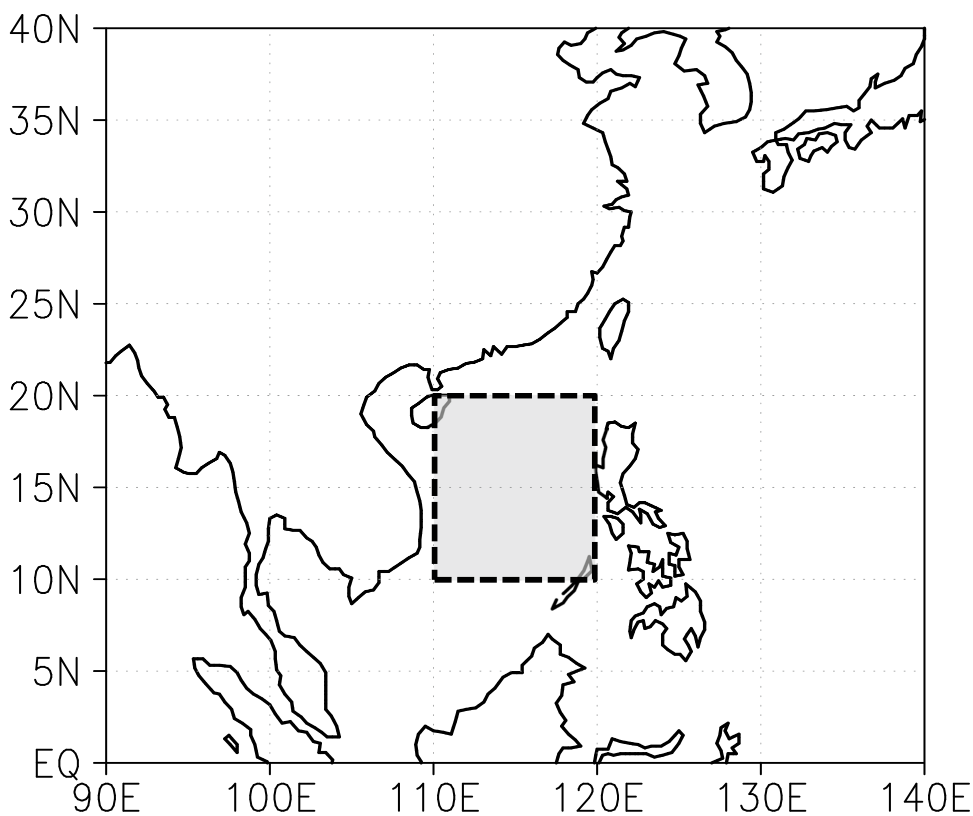

Fig. 1 The definition of South China Sea area (10°-20°N, 110°-120°E) in this study

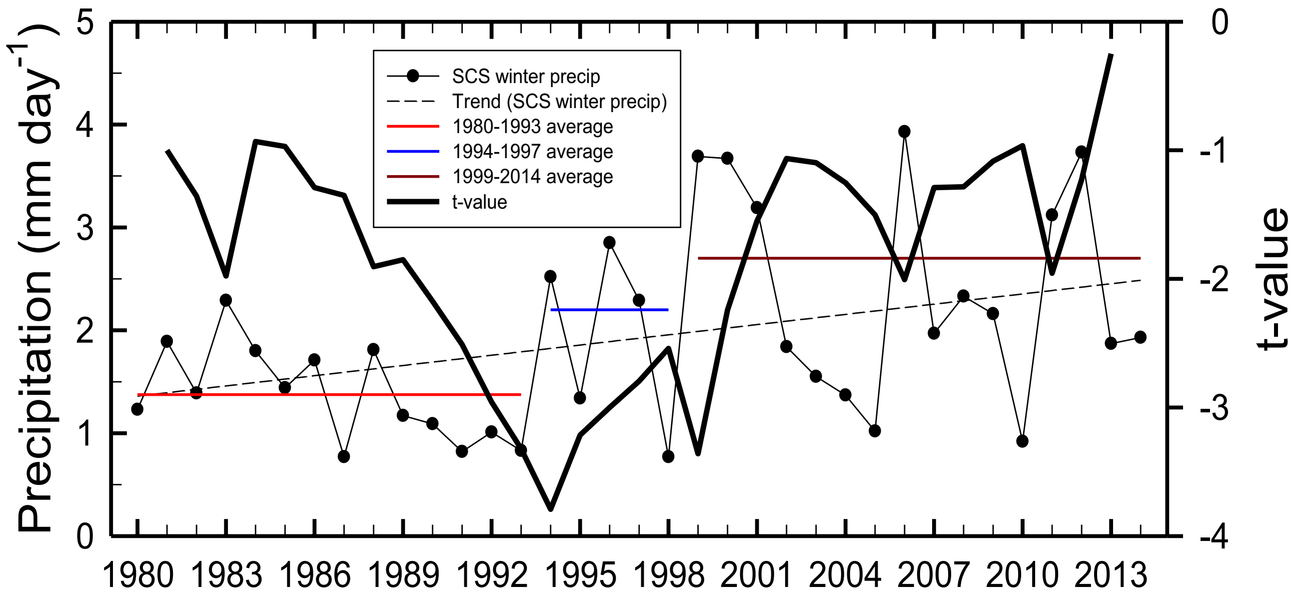

Fig. 2 Time series of South China Sea (SCS) winter (December to February) precipitation. Red, blue, and brown lines indicate averages for the periods of 1980–1993, 1994–1997, 1999–2014, respectively. Thick black line indicates t-value on the statistical change-point analysis. The dashed line denotes the trend of SCS winter precipitation by Mann-Kendall trend test

during those in 1980–1993, but less during summers and autumns. Two peaks in precipitable water occurred in mid-June and mid-August during 1980–1993, whereas only one peak was observed in early August during 1999–2014. The summer, which can be defined using precipitable water, was similar in the two study periods from the end of May to the end of September. Seasonal variation differences in precipitable water between 1994 and 2014 and 1980–1993 were greater in 1999–2014 from December to May, but greater in other months 1980–1993, except for July (Fig. 3b).

4.2 Large-Scale Environments

4.2.1 Large-Scale Atmospheric Circulations

Figure 4a shows winter precipitation differences between 1994 and 2014 and 1980–1993. Overall, positive anomalies were exhibited in the Maritime Continent and the SCS, whereas negative anomalies were observed along the equatorial Pacific, which is a typical spatial distribution of precipitation anomalies displayed during La Niña events. On the other hand, negative anomalies were observed in East Asia. The pattern of spatial distribution of precipitable water differences between the two periods was similar to that of precipitation differences (Fig. 4b). Positive anomalies were distinctively shown in the Maritime Continent and the SCS, whereas clear negative anomalies were evident in the tropical and subtropical central and eastern Pacific, and negative anomalies centered in South China were observed in East Asia.

Differences in 850 hPa stream flows between the two periods were analyzed to identify the cause of precipitation differences between 1994 and 2014 and 1980–1993 (Fig. 5a). Anomalous anticyclonic circulation was strengthened in the tropical eastern Pacific in both hemispheres, and anomalous cyclonic circulations were located on the western coast of Australia and the SCS. Anomalous easterlies (anomalous trade winds) were strengthened in the equatorial Pacific due to anomalous atmospheric circulations. Furthermore, anomalous westerlies and anomalous easterlies joined in the eastern sea of the Philippines and moved toward the SCS. Anomalous southerlies supplied anomalous warm and humid air to the SCS, causing an increase in SCS winter precipitation. In addition, anomalous southerlies and northeasterlies, directed away from the East-Asian continent combined in the SCS and increased SCS winter precipitation, and an anomalous west-high east-low pressure system, which is typical of the pressure system pattern in the winter season, formed in East Asia.

Differences in 200 hPa stream flows between 1994 and 2014 and 1980–1993 showed that anomalous cyclonic circulations were strengthened at the subtropical Pacific in both hemispheres (Fig. 5b). As a result, anomalous westerlies were formed in the equatorial Pacific, and anomalous southeasterlies were strengthened in the SCS due to the anomalous

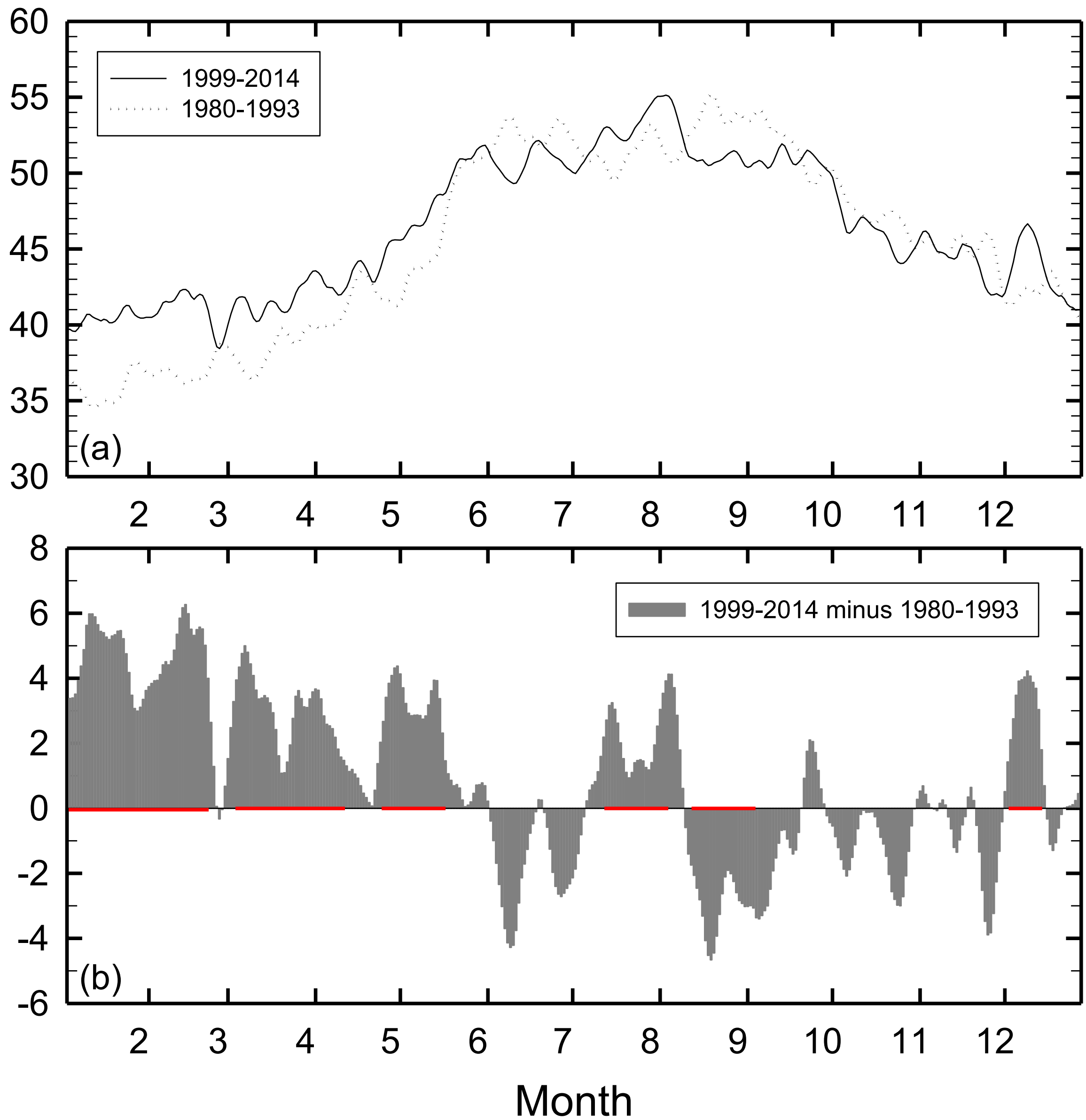

Fig. 3 Time series of the 7-day running averaged precipitable water over the SCS for the period (**a**) 1980–1993 (dotted line) and 1999–2014 (solid line), and (**b**) their epochal difference. In (**b**), red lines are significant at the 95% confidence level

cyclones, the centers of which were located in the western region of Australia and the southern region of China.

Since precipitation is more likely to increase as the air temperature anomaly in the lower troposphere increases, the difference between the atmospheric temperatures at the upper and lower tropospheres during the two periods was investigated (Fig. 6a and b). As shown in Fig. 6a, warm anomalies were formed in a southwest to northeast direction at the Aleutian Islands, which included the SCS in the lower troposphere. In contrast, cold anomalies were strengthened in the East-Asian continent and the equatorial central and eastern Pacific. Also, cold anomalies were strengthened in the analysis region, except for the East-Asian continent and Australia in the upper troposphere (Fig. 6b). Thus, positive anomalies were exhibited in the analysis region, except for the East-Asian continent, Australia, and the equatorial central and eastern Pacific, within the difference between air temperature anomalies in the lower and upper tropospheres (Fig. 6c), which meant these regions had higher air temperature anomalies in the lower troposphere than in the upper troposphere during 1999–2014. Furthermore, this spatial distribution was similar to that observed for precipitable water differences during 1994–2014 and 1980–1993, as mentioned above.

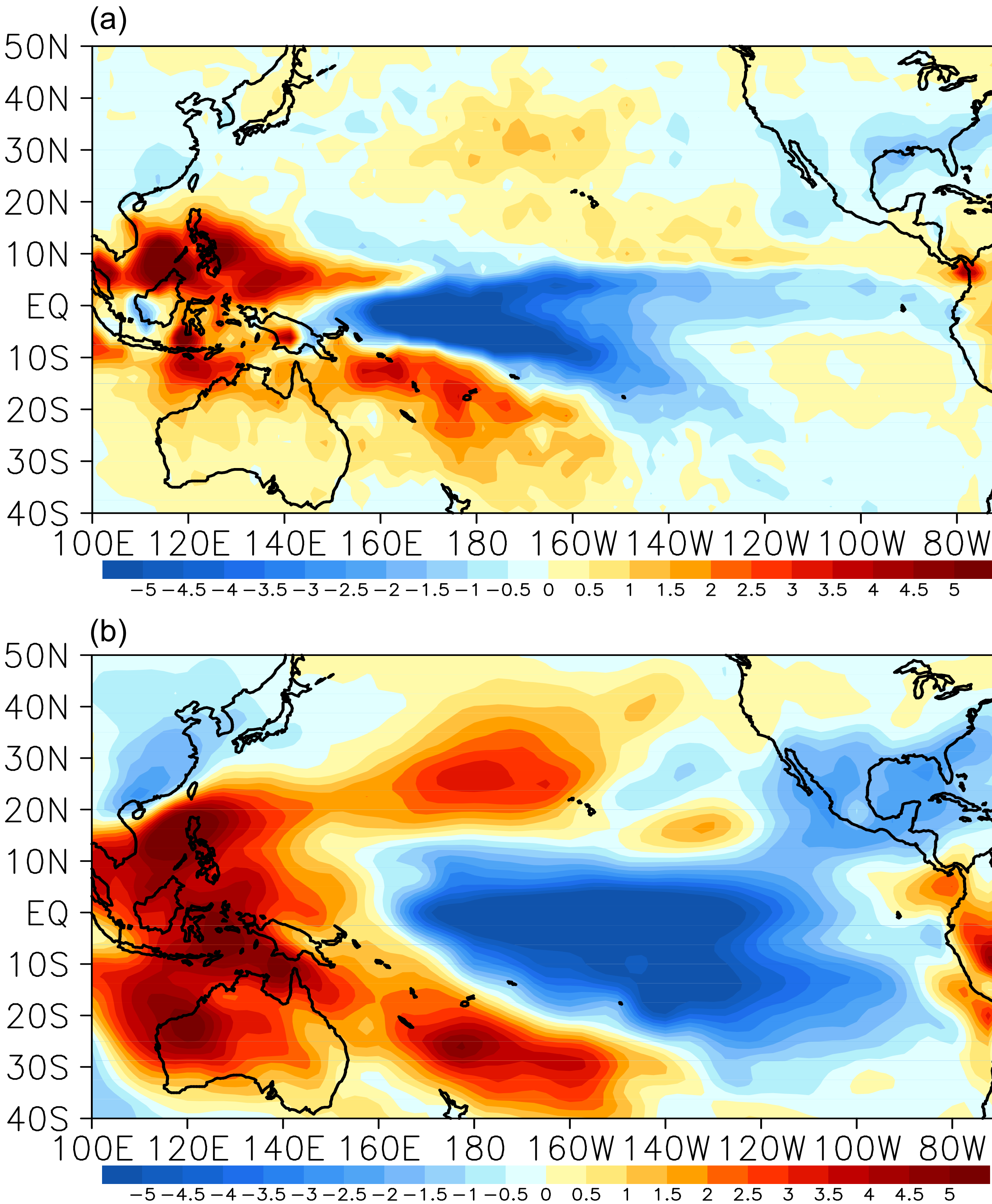

Fig. 4 Epochal differences (1999–2014 (9914) minus 1980–1993 (8093)) in the averaged (**a**) precipitation and (**b**) precipitable water

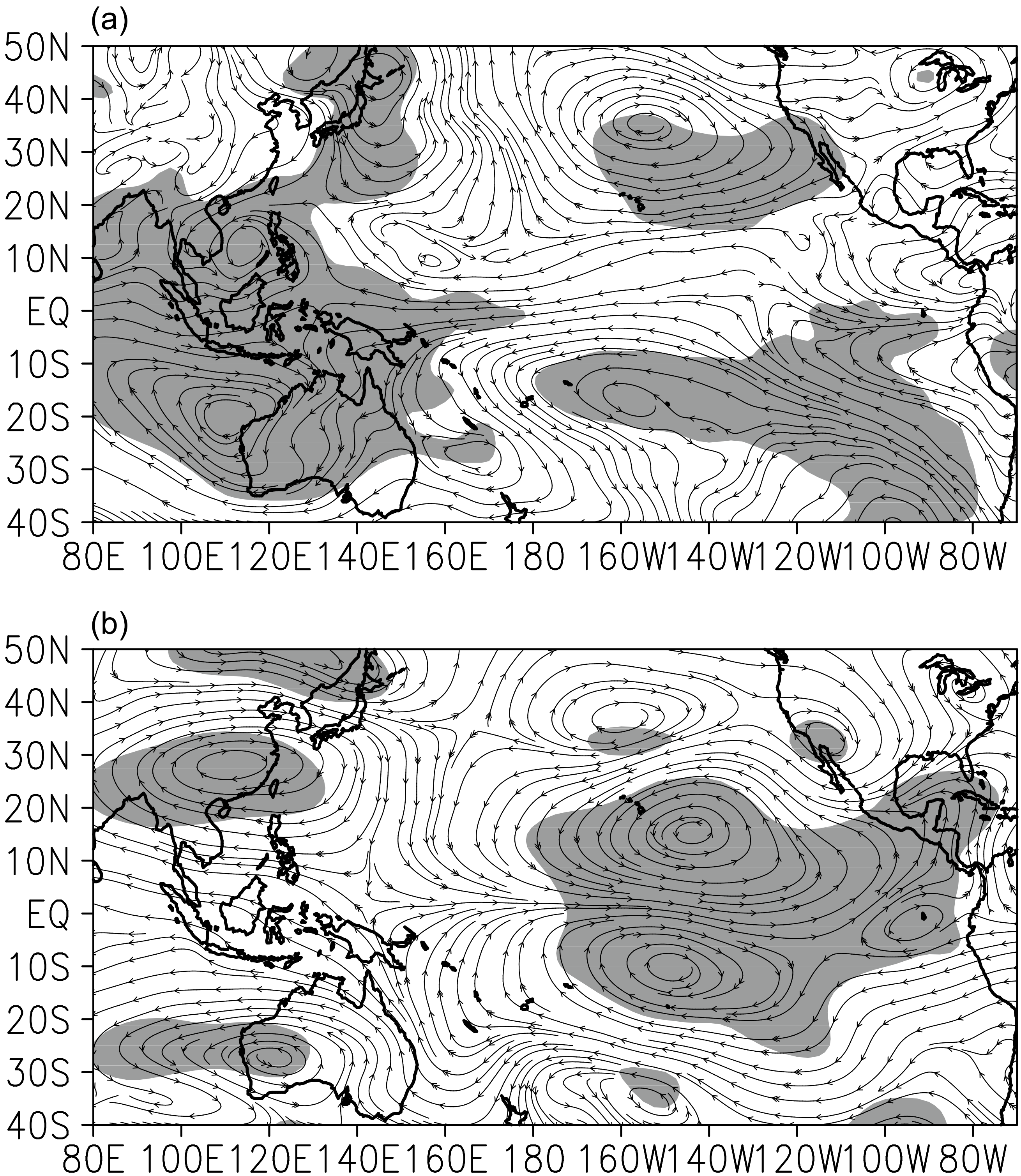

Fig. 5 Same as in Fig. 4., but for (**a**) 850 hPa stream flows and (**b**) 200 hPa stream flows. Shaded areas are significant at the 95% confidence level

850 and 200 hPa horizontal divergences were analyzed to identify differences in atmospheric circulation anomalies in upper and lower tropospheres during the two periods (Fig. 7). Regarding the 850 hPa horizontal divergence, negative anomalies were strengthened in the SCS, whereas positive anomalies were strengthened in the mid-latitude regions in East Asia, which includes northern China, Korea, and Japan (Fig. 7a). This implied that anomalous

Fig. 6 Same as in Fig. 4, but for (**a**) 850 hPa air temperature, (**b**) 200 hPa air temperature, and (**c**) their difference. Contour intervals are 0.4 °C for 850 hPa air temperature and 0.2 °C for 200 hPa air temperature. Shaded areas are significant above the 95% confidence level by *t*-test

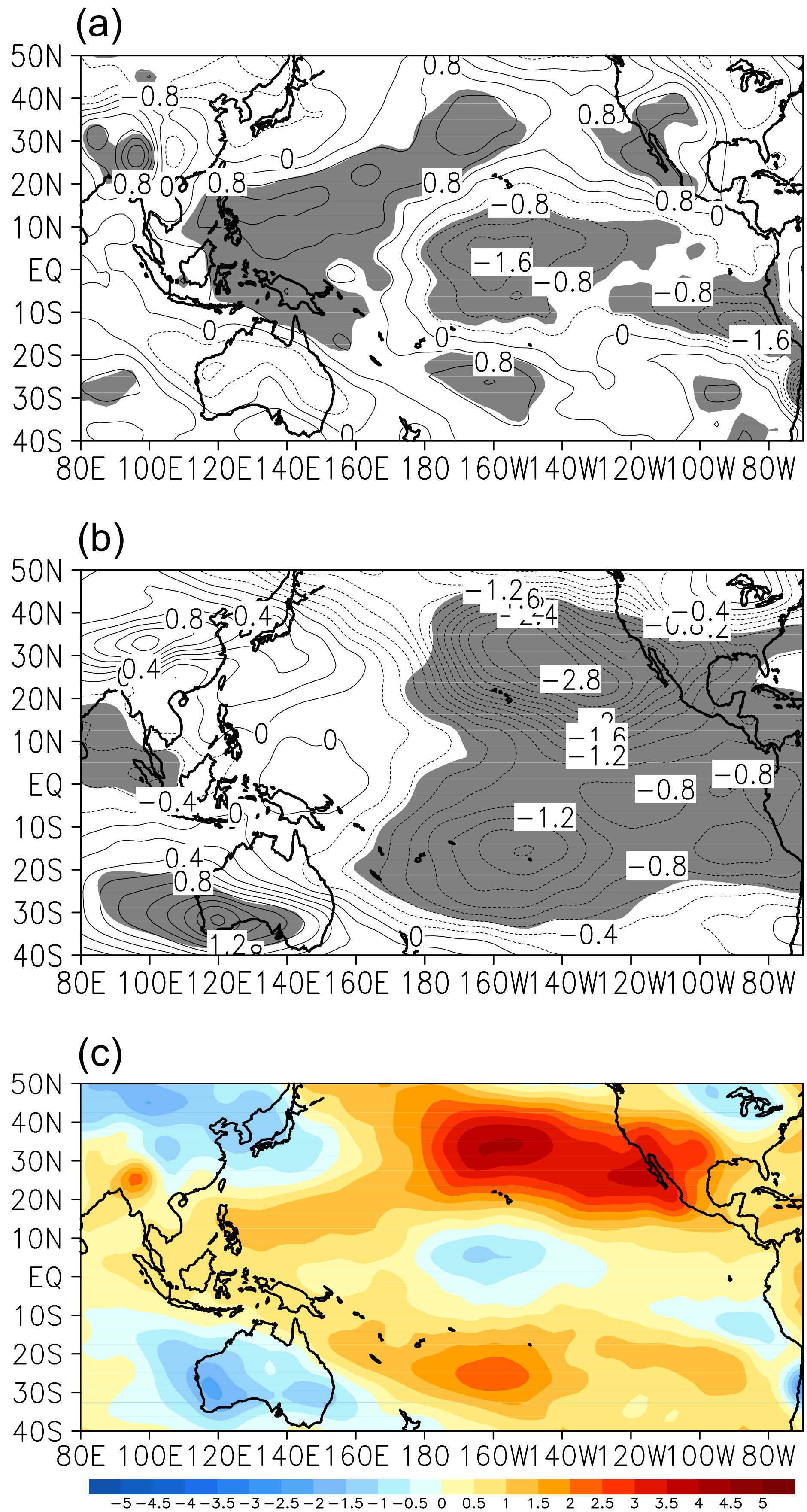

convergence was strengthened in the SCS in the lower troposphere during the 1999–2014 period, while anomalous divergence was strengthened in the mid-latitude region. According to our analysis of 200 hPa horizontal divergence, the centers of positive anomalies were located in the SCS, whereas negative anomalies were strengthened in the southern and northern regions of China and Japan. This indicated that anomalous divergence was strengthened in the SCS, whereas anomalous convergence was strengthened in the southern and northern regions of China and Japan in the upper troposphere during 1999–2014. Thus, based on considerations of upper and lower tropospheres, anomalous upward flows were strengthened in the SCS, and anomalous downward flows were strengthened in the mid-latitude East Asian region in the SCS during 1999–2014.

In order to confirm that anomalous upward flows were strengthened in the SCS and anomalous downward flows were strengthened in the mid-latitude region in East Asia during 1999–2014, differences between vertical meridional atmospheric circulations averaged over the 110°-120°E longitude band, including the SCS, were analyzed between the two periods (left panel of Fig. 8a). Strong anomalous upward flows were formed in the 0°-25°N latitude band, where the SCS was located, whereas anomalous downward flows were strengthened in the 30°-40°N latitude band, that is, a mid-latitude region in East Asia. Choi et al. (2016) demonstrated easterly vectors at 200 hPa from ascending vectors along 10°N and descending vectors along 25°N, which implied that the local Hadley circulation, whereby air ascends in the SCS and descends in the mid-latitude region in East Asia, was strengthened during 1999–2014. In fact, the ascent around 50°N contributed more to the descent along 30°-40°N.

Differences in the vertical distributions of air temperature during the two periods were also investigated. Warm anomalies deviated in a northerly direction from the lower troposphere at 10°-20°N, and thus, the centers of warm anomalies were located at 30°N in the upper troposphere (left panel of Fig. 8b). In contrast, cold anomalies were formed at mid-latitude in East Asia.

In addition, differences between the vertical distributions of specific humidity in 1994–2014 and 1980–1993 were examined. The results showed that positive anomalies were strengthened in the latitude band (0°-20°N) of the SCS, whereas negative anomalies were strengthened in the northern region above 20°N (left panel of Fig. 8c). Thus, anomalous warm and humid airs were strengthened in both upper and lower tropospheres in the SCS region during 1999–2014 while anomalous cold and dry airs were strengthened in the mid-latitude region in East Asia.

Regarding the characteristics of the anomalous vertical zonal atmospheric circulations, we analyzed average differences in vertical zonal atmospheric circulations over the 5°S to 20°N latitude band, including the SCS, during 1994–2014 and 1980–1993 (right panel of Fig. 8a). The results showed that anomalous upward flows were strengthened in regions west of 170°E, whereas anomalous downward flows were strengthened in regions east of 170°E. This implied that the Walker circulation, that is, ascent of air in the equatorial western Pacific and descent in the equatorial central and eastern Pacific, was strengthened in 1999–2014. Differences between vertical distributions of air temperatures in the two periods showed that warm anomalies were strengthened in regions west of 170°E, whereas cold anomalies were strengthened in regions east of 170°E (right panel of Fig. 8b).

Differences between the vertical distributions of specific humidities in the two periods showed that positive anomalies were strengthened in regions west of 170°E, whereas negative anomalies were strengthened in regions east of 170°E (right panel of Fig. 8c). Thus, anomalous warm and humid airs were strengthened in the equatorial western Pacific, including the SCS, whereas anomalous cold and dry airs were strengthened in the equatorial central and eastern Pacific in upper and lower tropospheres during 1999–2014. These patterns were typical anomalous vertical zonal atmospheric circulations and anomalous vertical environmental structures formed during La Niña events.

Differences between SSTs in 1994–2014 and 1980–1993 were analyzed to determine whether La Niña events were strengthened in 1999–2014 (Fig. 9). We found cold anomalies were strengthened in the equatorial central and eastern Pacific and on the west American coast, whereas warm anomalies were strengthened in other regions, which was typical of the spatial distribution of SSTs during La Niña events.

4.2.2 Interdecadal Variation of Indices and Global-Scale Atmospheric Circulations

We analyzed the time-series of the Niño-3.4 index and SCS winter precipitation to determine whether SCS winter precipitation was related to El Niño/the Southern Oscillation (ENSO; Fig. 10a). Niño-3.4 indices revealed a non-significant decreasing tendency. Interestingly, Niño-3.4 indices and SCS winter precipitation exhibited a clear out-of-phase relationship with a high negative correlation of −0.64, which was significant at the 99% confidence level and showed an inverse relationship existed between SST in the Niño-3.4 region (5°S to 5°N, 170°W to 120°W) and SCS winter precipitation.

Time-series of SCS winter precipitation and 850 hPa zonal wind indices averaged over the Niño-3.4 region (hereafter referred to as the U850 index) were also analyzed (Fig. 10b). Although not significant, the time series

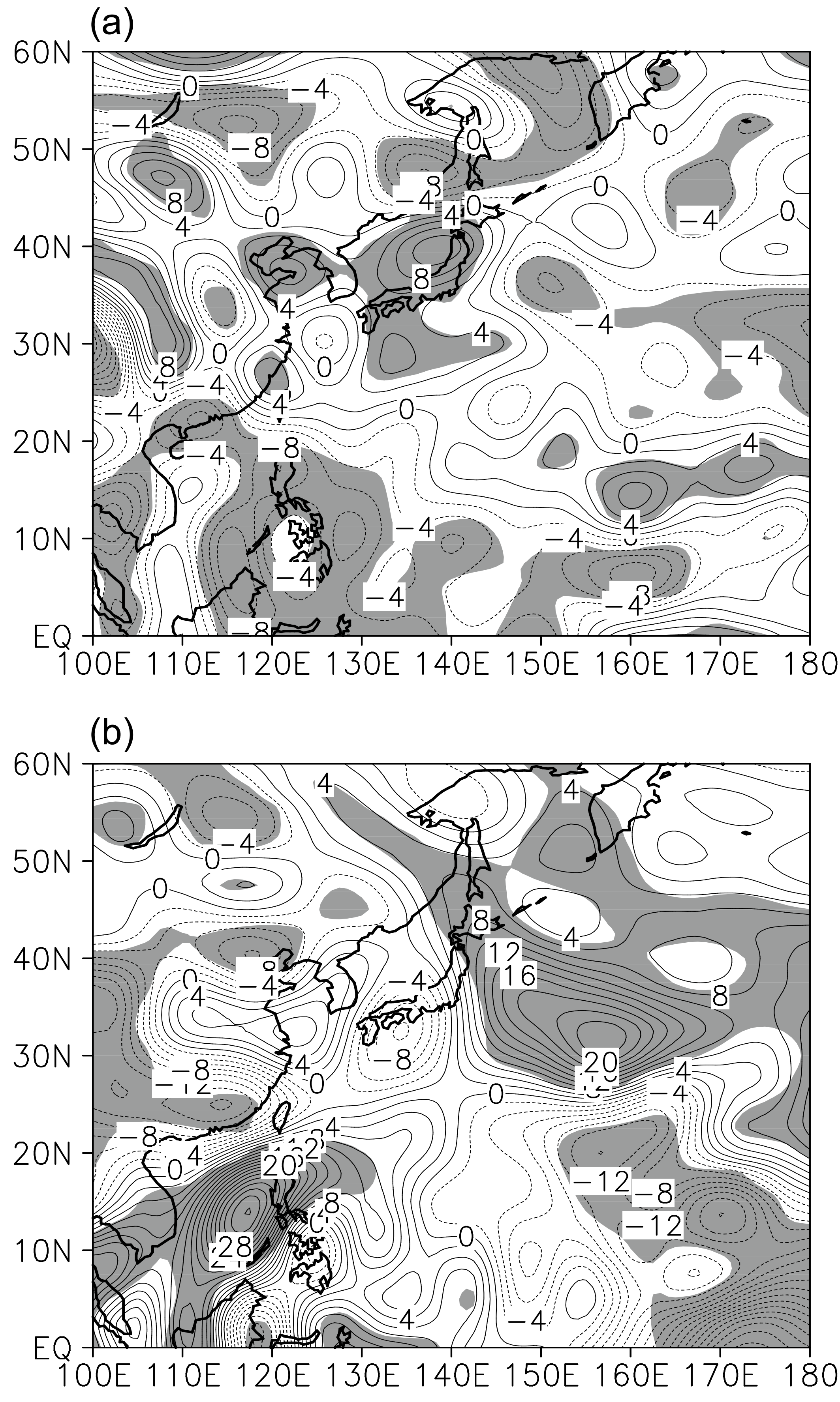
(a)
60N
50N
40N
30N
20N
10N
EQ
100E 110E 120E 130E 140E 150E 160E 170E 180
(b)
60N
50N
40N
30N
20N
10N
EQ
100E 110E 120E 130E 140E 150E 160E 170E 180

◂**Fig. 7** Same as in Fig. 4, but for (**a**) 850 hPa and (**b**) 200 hPa horizontal divergences. Shaded areas are significant above the 95% confidence level by *t*-test. Contour interval is 2 $s^{-1} \times 10^7$

of normalized U850 indices showed a decreasing trend, and a clear out-of-phase relationship was observed between the two variables with a high negative correlation of −0.60, which was significant at the 99% confidence level. This relation showed that if the 850 hPa zonal wind in the lower troposphere increased (decreased) in the Niño-3.4 region, SCS winter precipitation decreased (increased), which was consistent with the results obtained for differences in 850 hPa stream flows during 1994–2014 and 1980–1993 mentioned above.

When we analyzed the time-series of SCS winter precipitation and 200 hPa zonal wind indices (hereafter referred to as the U200 index) averaged over the Niño-3.4 region (Fig. 10c), the time series of normalized U200 indices showed an increasing overall trend, which was significant at the 90% confidence level. Furthermore, these two variables exhibited an in-phase relationship with a high positive correlation of 0.59 (significant at the 99% confidence level), which implied that if the 200 hPa zonal wind in the upper troposphere increased (decreased) in the Niño-3.4 region, SCS winter precipitation increased (decreased). This result was consistent with our analysis results of 200 hPa stream flow differences during the two periods, as analyzed above.

The combined zonal wind index, such as the difference in zonal wind indices between 200 hPa and 850 hPa, which physically reflects the variability in Walker circulation, was analyzed (Fig. 10d). The combined zonal wind index and SCS winter precipitation show a good relationship.

Because our analysis showed that the anomalous east-high west-low pressure pattern was strengthened during winter in East-Asian regions in 1999–2014, and that this resulted in increased precipitation in the SCS, we examined time series of winter SCS precipitation and EAWM indices (Fig. 11) Overall, EAWM indices exhibited a non-significant increasing tendency (thick dotted line). Furthermore, the two time series exhibited an in-phase relationship, which had a positive correlation of 0.48 and was significant at the 99% confidence level. This meant that as the EAWM strengthened (weakened), winter precipitation in the SCS increased (decreased). Rudeva and Simmonds (2015) presented a global analysis of frontal activity variability, derived from ERA-Interim data over a 34-year period from January 1979 to March 2013, performed using a state-of-the-art frontal tracking scheme. In December to February over this epoch, a northward shift of frontal activity occurred in the Pacific in the Northern Hemisphere (NH), whereas in the Southern Hemisphere (SH), largest trends were identified in the austral summer and frontal activity exhibited a southward shift over the Southern Ocean. Enhancement of the local Hadley circulation, with ascent over the equatorial region and descent over mid-latitudes is an important issue. Anomalous northerlies/northeasterlies were apparent over the SCS (Fig. 5a), which indicated that the strength of the EAWM is influenced by a pressure gradient between the equatorial region (low pressure) and the mid-latitude region (Siberian high) (Wang and Chen 2014; Olaguera et al. 2018).

To determine the cause of EAWM strengthening and the anomalous west-high east-low pressure pattern in East-Asian regions during 1999–2014, we investigated differences in Water Equivalents of Accumulated Snow Depth (WEASDs) between the two periods (Fig. 12). Anomalous snow affects the thermal state of the land surface and overlying air due to snow-albedo and snow-hydrological effects (Barnett et al. 1989). Positive anomalies were more evident in the 20°-50°N mid-latitude region in East Asia rather than in high latitude regions above 50°N. Notably, positive anomalies were seen even in the southern regions of China. Snow cover lowers ground temperatures, reflects solar energy, and cools surrounding air temperatures when the snow melts, which causes local and remote atmospheric circulation changes. Due to these effects of snowfall, an anomalous west-high east-low pressure pattern could have been strengthened in East-Asian regions during 1999–2014 where WEASDs were high.

We also investigated whether the indices related to changes in SCS winter precipitation mentioned above (850 and 200 hPa zonal winds averaged over the Niño-3.4 region and EAWM indices) also revealed interdecadal variation (Fig. 13). The 850 hPa zonal wind averaged over the Niño-3.4 region during 1980–1993 was 0.44, whereas that during 1999–2014 was −0.48, and this difference was significant at the 95% confidence level. The 200 hPa zonal wind averaged over the Niño-3.4 region during 1980–1993 was −0.38 and during 1999–2014 was 0.53, and this difference was also significant at the 95% confidence level. Average EAWM indices during 1980–1993 and 1999–2014 were − 0.40 and 0.17, respectively, which was also a significant difference at the 90% confidence level. Thus, interdecadal variations, in which the winter precipitation increased since 1999 across the SCS, were evident in indices related to changes in winter precipitation in the SCS.

Differences between 850 hPa and 200 hPa velocity potentials during the two periods were analyzed to identify differences between the characteristics of global-scale atmospheric circulation in the two periods (Fig. 14). For 850 hPa velocity potential, the centers of negative anomalies were located in the Maritime Continent, whereas the centers of positive anomalies were located in the equatorial eastern Pacific (Fig. 14a). This implied that anomalous convergence developed in the Maritime Continent, including the SCS, whereas anomalous divergence was strengthened in the equatorial eastern Pacific in the lower troposphere during

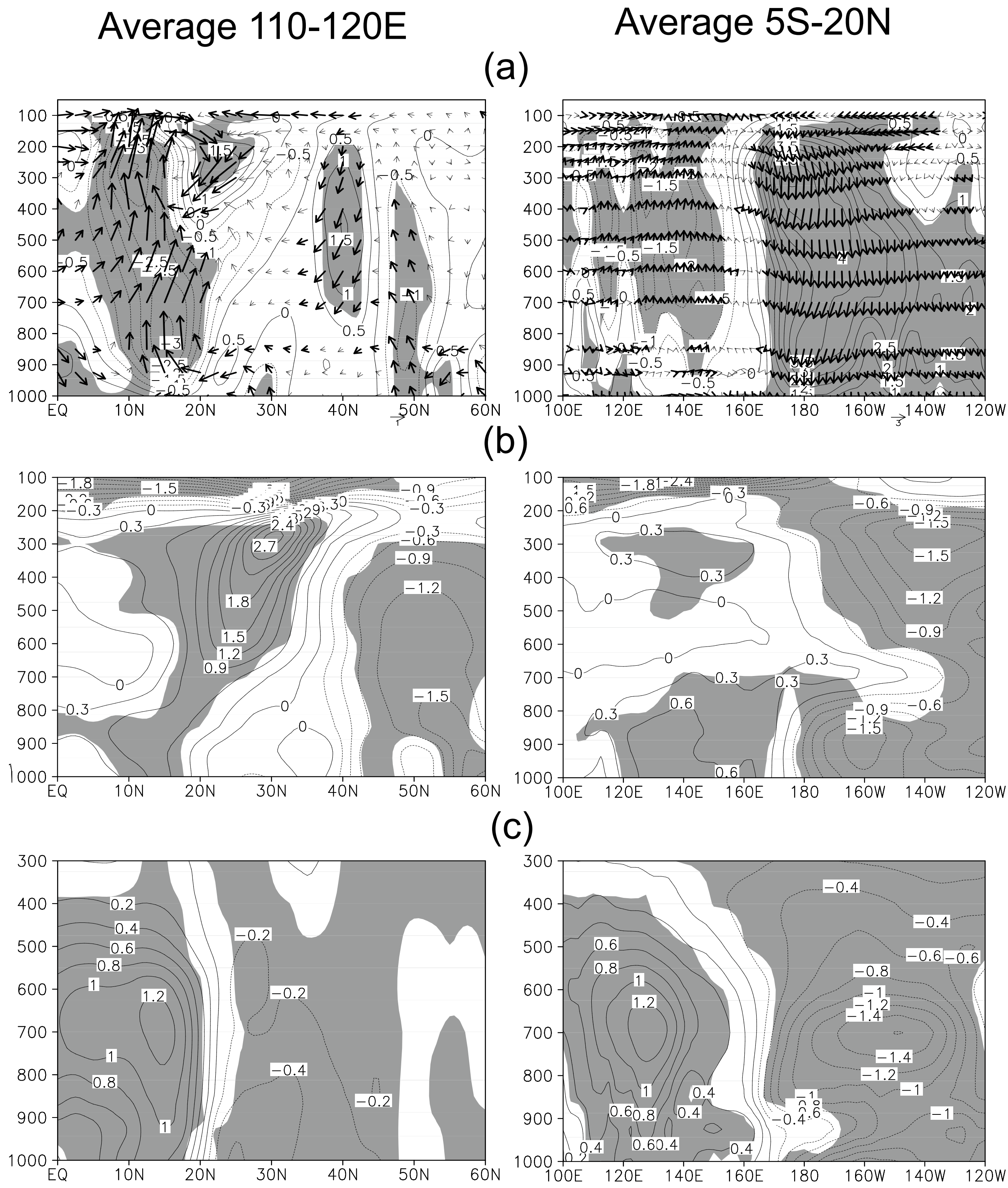

Fig. 8 Composite differences of latitude–pressure and longitude-pressure cross sections of (**a**) vertical velocity (contours) and meridional circulations (vectors), (**b**) air temperature, and (**c**) specific humidity averaged along 110°-120°E and 5°S-20°N between 9914 and 8093 for December–February, respectively. The values of vertical velocity are multiplied by −100. Bold arrows and shaded areas are significant above the 95% confidence level by *t*-test. Contour intervals are 0.5^{-2} hPa s^{-1} for vertical velocity, 0.3 °C for air temperature, and 0.2 g kg^{-1} for specific humidity, respectively

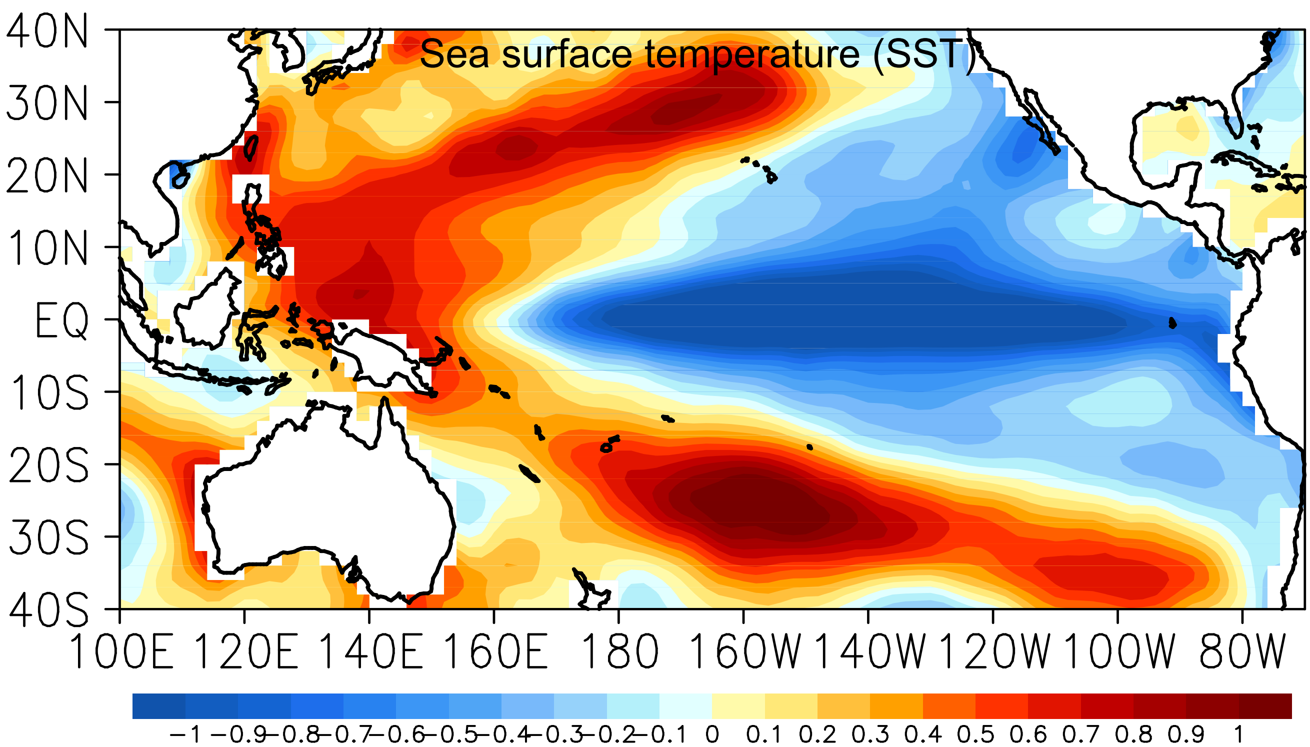

Fig. 9 Same as in Fig. 4, but for sea surface temperature (SST)

1999–2014. The spatial distribution at the 200 hPa velocity potential showed a spatial distribution pattern complementary to that at the 850 hPa velocity potential (Fig. 14b), indicating anomalous divergence had developed in the Maritime Continent, including the SCS, and that anomalous convergence had strengthened in the equatorial eastern Pacific in the upper troposphere during 1999–2014. In summary, considering upper and lower tropospheres, these results showed that the Walker circulation, whereby air ascended from the Maritime Continent, including the SCS and descended at the equatorial eastern Pacific, was strengthened during 1999–2014.

5 Summary and Conclusion

This study shows that average winter precipitation has increased across the SCS since 1999. To determine the cause of this increase, we analyzed the differences between averages in 1994–2014 and 1980–1993. As regards seasonal variations in precipitation, the summer wet season remained unchanged from the end of May to the end of September during both study periods. However, during 1999–2014 precipitation tended to be less during summer and autumn and more during winter and spring than in 1980–1998.

Spatial distributions of winter precipitation differences between the two periods showed that negative anomalies were distributed from the equatorial eastern Pacific to the equatorial central Pacific, and that positive anomalies were distributed in the subtropical western Pacific, the Maritime Continent, and the northern part of Australia, which is typical of the spatial distribution of precipitation anomalies displayed during La Niña events. On the other hand, most northern parts above 20°N in East Asia showed negative anomalies centered over South China.

To determine the characteristics of large-scale atmospheric circulations that caused the different spatial distributions of precipitation during 1994–2014 and 1980–1993, we investigated differences between 850 hPa stream flows during the two periods. Anomalous anticyclonic circulations were strengthened in the central and eastern Pacific, and due to these anomalous circulations, anomalous easterlies (anomalous trade winds) were strengthened in the equatorial Pacific. In contrast, a pair of anomalous cyclonic circulations were formed in the Australian western sea and the SCS. Thus, anomalous southeasterlies and anomalous northeasterlies conjoined in the SCS. These anomalous circulations are typical of La Niña events. Furthermore, as discussed earlier, negative precipitation anomalies were formed from the equatorial eastern Pacific to the equatorial central Pacific, whereas positive precipitation anomalies were strengthened in the subtropical western Pacific, the Maritime Continent, and northern parts of Australia. On the other hand, an anomalous west-high east-low pressure system, which is

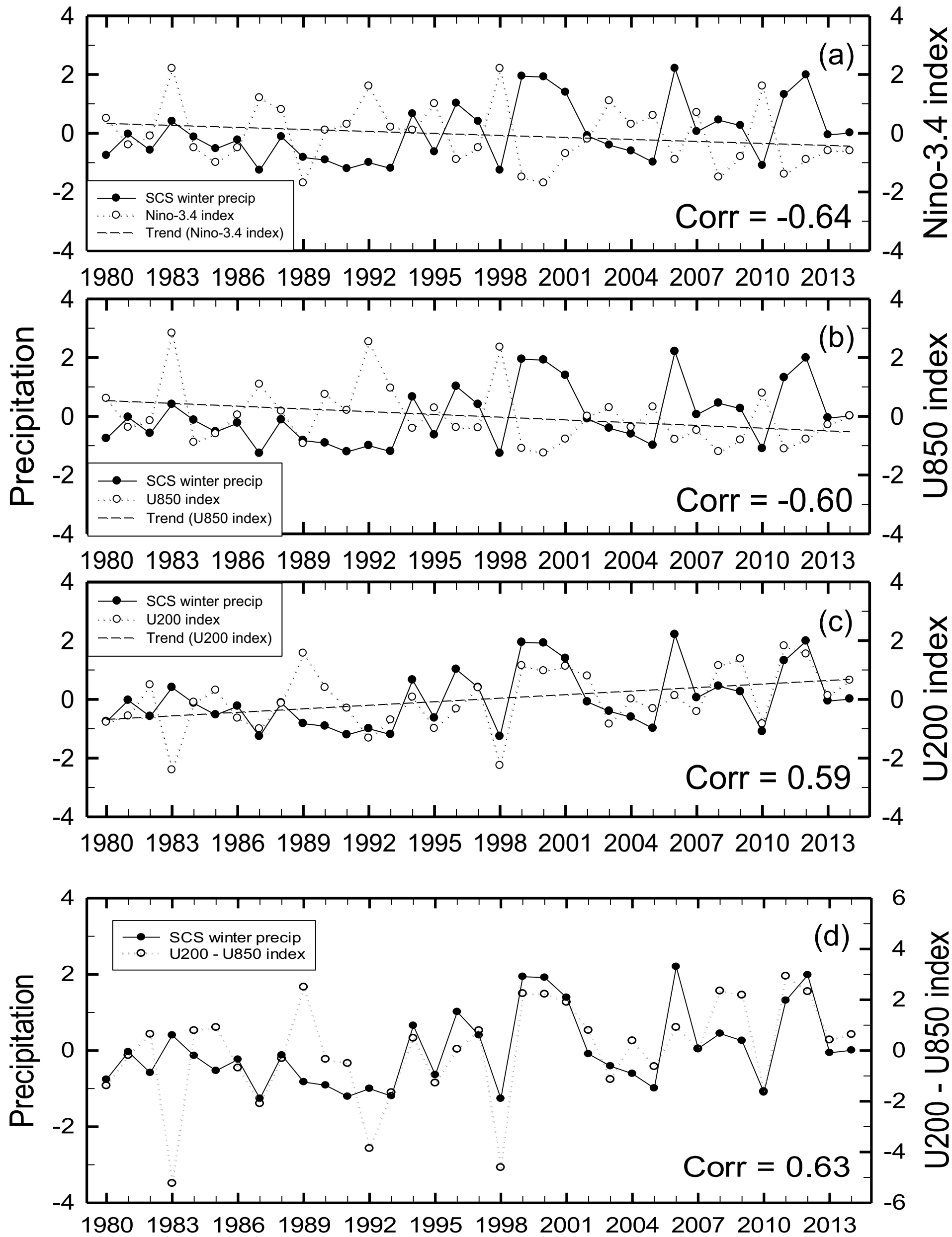

Fig. 10 Time series of (**a**) SCS winter precipitation (solid line with a closed circle) and Niño-3.4 index and (**b**) SCS winter precipitation and normalized winter 850 hPa zonal wind (dotted line with an open circle) averaged over Niño-3.4 region (5°S-5°N, 170°W-120°W), (**c**) SCS winter precipitation and normalized winter 200 hPa zonal wind (dotted line with an open circle) averaged over Niño-3.4 area, (d) SCS winter precipitation and normalized winter zonal wind difference between 200 hPa and 850 hPa (dotted line with an open circle) averaged over Niño-3.4 area, and trends of Niño-3.4 index, normalized winter 850 hPa zonal wind, and normalized winter 200 hPa zonal wind by Mann-Kendall trend test

a typical pressure system pattern observed in winter, was strengthened in East-Asian regions. Thus, anomalous northerlies were strengthened in most East Asian regions, and as a result, negative precipitation anomalies were created in most regions of the northern sector above 20°N in East Asia.

To determine whether La Niña events actually strengthened between the 1994–2014 and 1980–1993 study periods, differences in average zonal atmospheric circulations over the 5°S to 20°N region during winter were analyzed. Our results showed that anomalous upward flows were strengthened in regions west of 170°E, whereas anomalous downward flows were strengthened in the regions east of 170°E, which indicated the Walker circulation was stronger in 1994–2014 than in 1980–1993.

The analysis of averaged meridional atmospheric circulations over the longitude band 110°-120°E, which included the SCS, over the two periods showed that anomalous upward flows were strengthened in the SCS, and anomalous downward flows were strengthened in the mid-latitude region in East Asia, which showed the local Hadley circulation, that is, ascending air in the SCS and descending air at mid-latitude in East Asia, was stronger in 1999–2014.

The observed characteristics of large-scale atmospheric circulations associated with the causes of winter precipitation increased after 1999 in South China (Fig. 15), and the observation that SSTs during the two periods showed a typical La Niña pattern. Therefore, we further analyzed

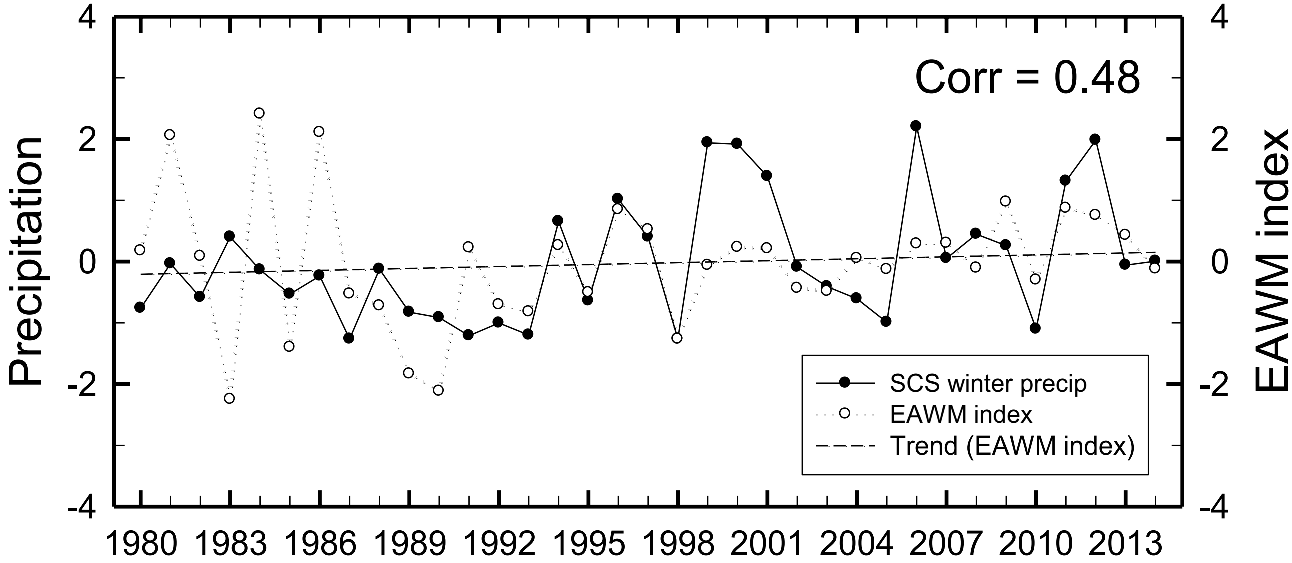

Fig. 11 Time series of (**a**) SCS winter precipitation (sold line with a closed circle) and East Asian winter monsoon (EAWM) index (dotted line with an open circle) averaged over 30°-45°N, 125°-145°E using 500 hPa geopotential height (Sun and Sun 1995), and the trend of EAWM index by Mann-Kendall trend test (dashed line)

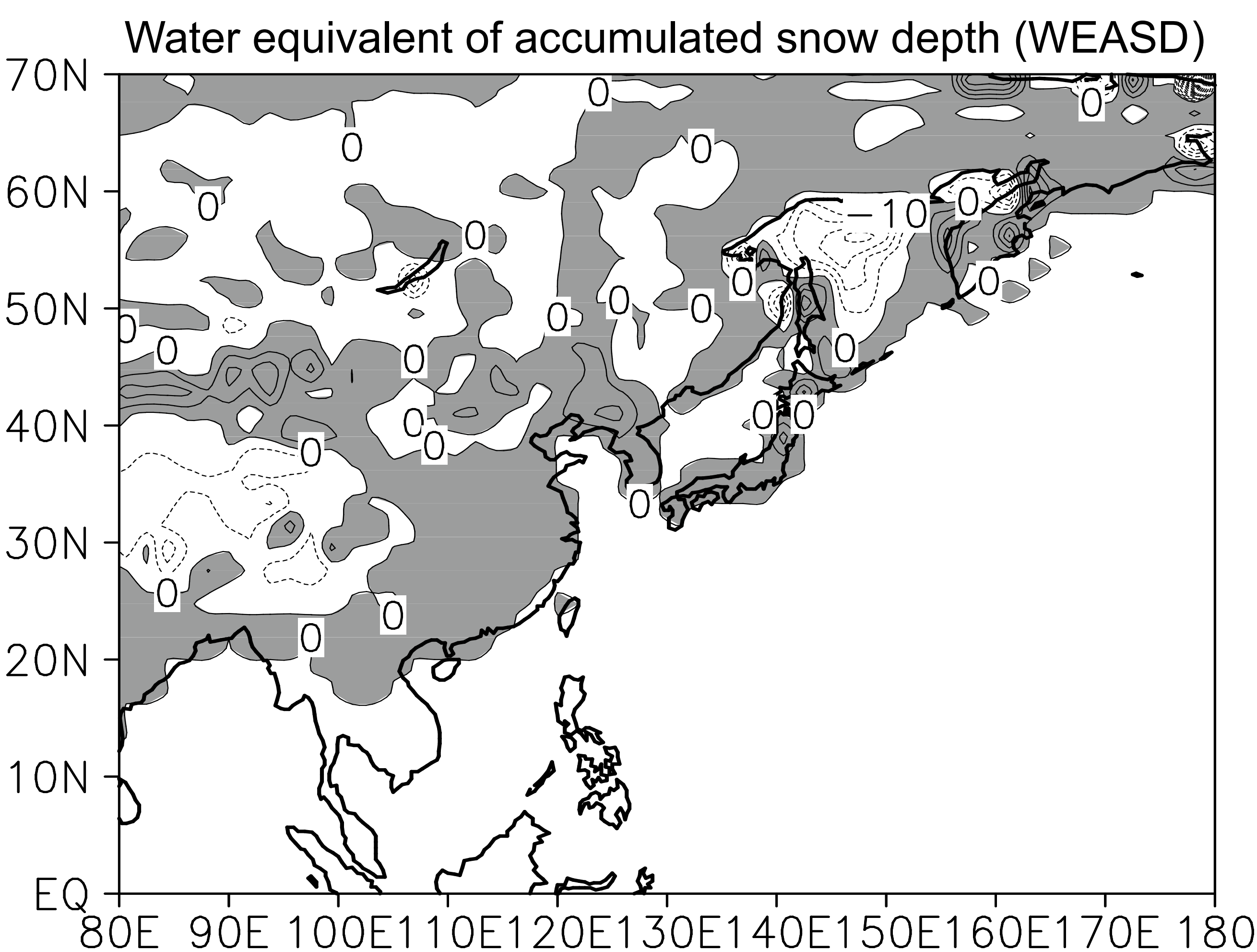

Fig. 12 Same as in Fig. 4, but for water equivalent of accumulated snow depth (WEASD). Contour inter is 10 kgm^{-2}. Shaded areas are positive values

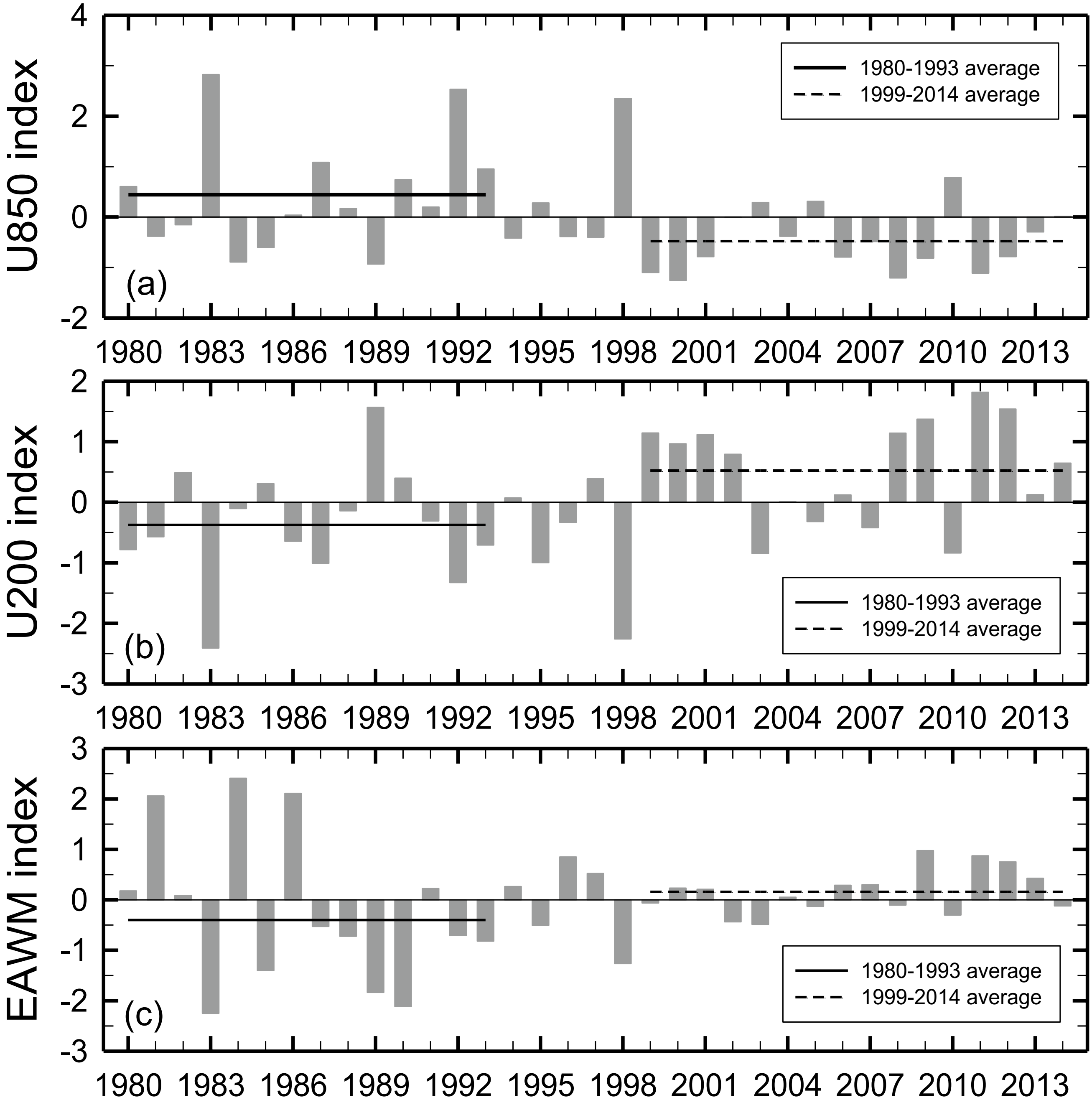

Fig. 13 Interdecadal variation of (**a**) normalized winter 850 hPa zonal wind averaged over Niño-3.4 region, (**b**) normalized winter 200 hPa zonal wind averaged over Niño-3.4 region, and (**c**) EAWM index

correlations between average SCS winter precipitations, Niño-3.4 indices, and 850 hPa and 200 hPa zonal winds over the Niño-3.4 region. SCS winter precipitation was found to be strongly and negatively correlated with Niño 3.4 SST indices, negatively correlated with 850 hPa zonal wind indices, and positively correlated with 200 hPa zonal wind indices, which suggested that SCS winter precipitation is positively related to Walker circulation intensity.

Because anomalous a west-high east-low pressure pattern in East-Asian regions during winters in 1999–2014 was strengthened and precipitation in the SCS was reduced, we analyzed the correlation between winter precipitation and

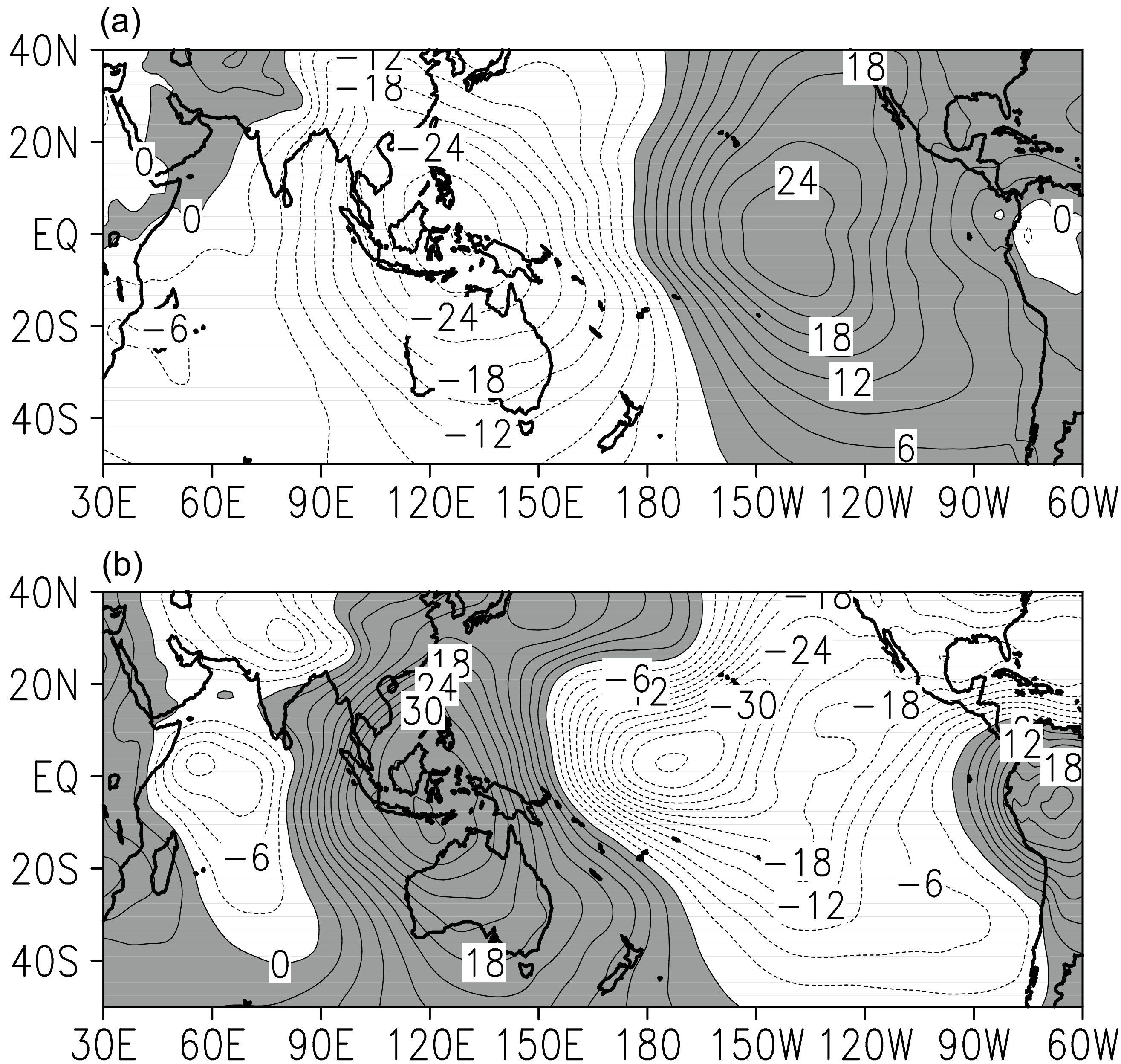

Fig. 14 Same as in Fig. 4, but for (**a**) 850 hPa and (**b**) 200 hPa velocity potential. Shaded areas denote negative anomalies. Contour interval is 3 $m^2s^{-1}10^{-6}$

EAWM indices in the SCS and found the two variables exhibited a positive correlation of 0.48. To determine the causes of EAWM strengthening and the anomalous west-high east-low pressure pattern in the East-Asian regions during 1999–2014, we examined differences between Water Equivalents of Accumulated Snow Depth (WEASDs) in the two periods. Positive anomalies were more obvious in the 20°-50°N mid-latitude region than in high latitude regions above 50°N in East Asia, and notably, positive anomalies were seen even in the southern regions of China.

This study showed that indices related to changes in winter precipitation in the SCS (Niño-3.4 indices, 850 hPa and 200 hPa zonal winds averaged over the Niño-3.4 region, and EAWM indices) exhibit interdecadal variations. In addition, these indices were found to be the causes of interdecadal variations in SCS winter precipitation. Differences between 850 and 200 hPa velocity potentials in the two study periods were analyzed to identify the characteristics of global-scale atmospheric circulation during the two periods. Furthermore, based on considerations of upper and

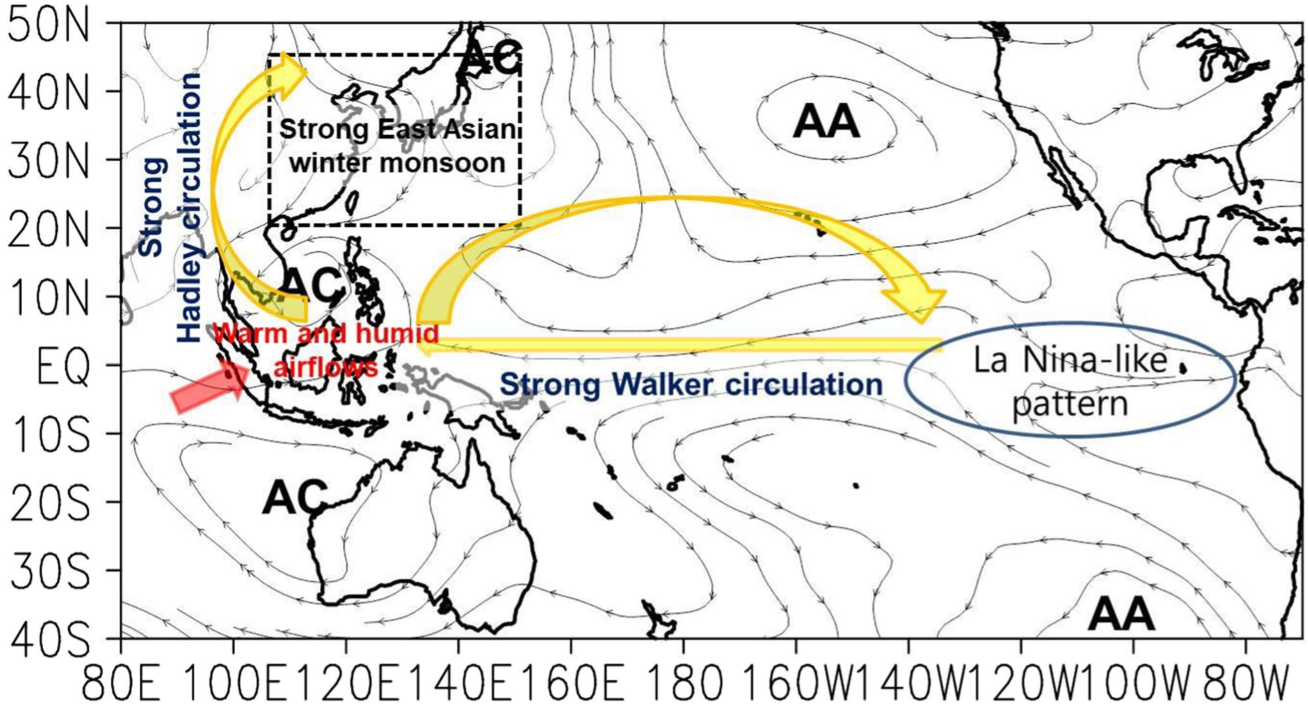

Fig. 15 Schematic illustration of anomalous atmospheric circulation changes on the recent decrease of SCS winter precipitation. Abbreviations of 'AC' and 'AA' indicate 'anomalous cyclone' and 'anomalous anticyclone', respectively

lower tropospheres, the Walker circulation was found to be stronger in 1999–2014 than in 1980–1993.

Observations around SCS, especially in South China, show that summer monsoon rainfall is increasing (Preethi et al. 2017a). In addition, climate model simulations and projections also showed that summer monsoon rainfall has increased in SCS and will continue to increase, respectively (Preethi et al. 2017b). In this respect, further research on the issue is needed in the future.

Acknowledgements This study was carried out with the support of the Cooperative Research Program for Agriculture Science and Technology Development (Project No. PJ01489102) of the Rural Development Administration, Republic of Korea.

References

Barnett, T.P., Dumenil, L., Schlese, U., Roekler, E., Latif, M.: The effect of Eurasian snow cover on regional and global climate variations. J. Atmos. Sci. **46**, 661–686 (1989)

Centurioni, L.R., Niiler, P.N., Lee, D.K.: Near surface circulation in the South China Sea during the winter monsoon. Geophys. Res. Lett. **36**, L06605 (2009)

Chen, J.M., Chang, C.P., Li, T.: Annual cycle of the South China Sea surface temperature using the NCEP/NCAR reanalysis. J. Meteor. Soc. Japan. **81**, 879–884 (2003)

Choi, J.W., Lee, S.W., Lim, B.H., Kim, B.J.: Interdecadal change of winter precipitation over southern China in later 1990s. J. Meteor. Soc. Japan. **94**, 197–213 (2016)

Chu, P.S.: Large-scale circulation features associated with decadal variations of tropical cyclone activity over the central North Pacific. J. Clim. **15**, 2678–2689 (2002)

Chu, P.C., Edmons, N.L., Fan, C.W.: Dynamical mechanisms for the South China Sea seasonal circulation and thermohaline variabilities. J. Phys. Oceanogr. **29**, 2971–2989 (1999)

Delworth, T.L., Mann, M.E.: Observed and simulated multidecadal variability in the northern hemisphere. Clim. Dyn. **16**, 661–676 (2000)

Deser, C., Alexander, M.A., Xie, S.P., Phillips, A.S.: Sea surface temperature variability: patterns and mechanisms. Annu. Rev. Mar. Sci. **2**, 115–143 (2010)

Ding, Y.H.: Summer monsoon precipitations in China. J. Meteor. Soc. Japan. **70**, 373–396 (1992)

Elsner, J.B., Jagger, T., Niu, X.F.: Changes in the rates of North Atlantic major hurricane activity during the 20th century. Geophys. Res. Lett. **27**, 1743–1746 (2000)

He, Z., Wu, R.: Coupled seasonal variability in the South China Sea. J. Oceanogr. **69**, 57–69 (2012)

Ho, C.H., Baik, J.J., Kim, J.H., Gong, D.Y.: Interdecadal changes in summertime typhoon tracks. J. Clim. **17**, 1767–1776 (2004)

Hu, J.Y., Kawamura, H., Hong, H.S., Qi, Y.Q.: A review on the currents in the South China Sea: seasonal circulation, South China Sea warm current and Kuroshio intrusion. J. Oceanogr. **56**, 607–624 (2000)

Huang, B., Banzon, V.F., Freeman, E., Lawrimore, J., Liu, W., Peterson, T.C., Smith, T.M., Thorne, P.W., Woodruff, S.D., Zhang, H.M.: Extended Reconstructed Sea surface temperature version 4 (ERSST.v4): part I. Upgrades and intercomparisons. J. Clim. **28**, 911–930 (2014)

Kajikawa, Y., Bin, W.: Interdecadal change of the South China Sea summer monsoon onset. J. Clim. **25**, 3207–3218 (2012)
Kajikawa, Y., Yasunari, T., Wang, B.: Decadal change in intraseasonal variability over the South China Sea. Geophys. Res. Lett. **36**, L06810 (2009). https://doi.org/10.1029/2009gl037174
Kalnay, E., Kanamitsu, M., Kistler, R., et al.: The NCEP/NCAR 40-year reanalysis project. Bull. Amer. Meteor. Soc. **77**, 437–471 (1996)
Kistler, R., Kalnay, E., Collins, W., et al.: The NCEP–NCAR 50-year reanalysis: monthly means CD-ROM and documentation. Bull. Amer. Meteor. Soc. **82**, 247–267 (2001)
Lau, K.M., Ding, Y., Wang, J.T., Johnson, R., Keenan, T., Cifelli, R., Gerlach, J., Thiele, O., Rickenbach, T., Tsay, S.C., Lin, P.H.: A report of the field operations and early results of the South China Sea Mon soon experiment (SCSMEX). Bull. Amer. Meteor. Soc. **81**, 1261–1270 (2000)
Lestari, R.K., Watanabe, M., Kimoto, M.: Role of air-sea coupling in the interannual variability of the South China Sea summer monsoon. J. Meteor. Soc. Japan. **89A**, 283–290 (2011)
Liu, W.T., Xie, X.S.: Spacebased observations of the seasonal changes of south Asian monsoons and oceanic responses. Geophys. Res. Lett. **26**, 1473–1476 (1999)
Liu, Q.Y., Yang, H.J., Liu, Z.Y.: Seasonal feature of the Sverdrup circulation in the South China Sea. Prog. Nat. Sci. **11**, 202–206 (2001a)
Liu, Z., Yang, H., Liu, Q.: Regional dynamics of seasonal variability in the South China Sea. J. Phys. Oceanogr. **31**, 272–284 (2001b)
Liu, Q.Y., Jiang, X., Xie, S.P., Liu, W.T.: A gap in the indo-Pacific warm pool over the South China Sea in boreal winter: seasonal development and interannual variability. J. Geophys. Res. **109**, C07012 (2004)
Liu, W., Huang, B., Thorne, P.W., Banzon, V.F., Zhang, H.M., Freeman, E., Lawrimore, J., Peterson, T.C., Smith, T.M., Woodruff, S.D.: Extended Reconstructed Sea surface temperature version 4 (ERSST.v4): part II. Parametric and structural uncertainty estimations. J. Clim. **28**, 931–951 (2014)
Meehl, G.A., Hu, A.: Megadroughts in the Indian monsoon region and Southwest North America and a mechanism for associated multidecadal Pacific Sea surface temperature anomalies. J. Clim. **19**, 1605–1623 (2006)
Murakami, T., Matsumoto, J.: Summer monsoon over the Asian continent and western North Pacific. J. Meteor. Soc. Japan. **72**, 719–745 (1994)
Olaguera, L.M., Matsumoto, J., Kubota, H., Inoue, T., Cayanan, E.O., Hilario, F.D.: Interdecadal shifts in the winter monsoon rainfall of the Philippines. Atmosphere. **464** (2018)
Power, S., Casey, T., Folland, C., Colman, A., Mehta, V.: Inter-decadal modulation of the impact of ENSO on Australia. Clim. Dyn. **15**, 319–324 (1999)
Preethi, B., Mujumdar, M., Kripalani, R.H., Prabhu, A., Krishnan, R.: Recent trends and teleconnections among south and east Asian summer monsoons in a warming environment. Clim. Dyn. **48**, 2489–2505 (2017a). https://doi.org/10.1007/s00382-016-3218-0
Preethi, B., Mujumdar, M., Prabhu, A., Kripalani, R.H.: Variability and teleconnections of south and east Asian summer monsoon in present and future projections of CMIP5 climate models. Asia-Pac. J. Atmos. Sc. **53**(2), 305–325 (2017b). https://doi.org/10.1007/s13143-017-0034-3
Qu, T.D.: Role of ocean dynamics in determining the mean seasonal cycle of the South China Sea surface temperature. J. Geophys. Res. **106**, 6943–6955 (2001)
Rudeva, I., Simmonds, I.: Variability and trends of global atmospheric frontal activity and links with large-scale modes of variability. J. Clim. **28**, 3311–3330 (2015)
Shaw, P.T., Chao, S.Y.: Surface circulation in the South China Sea. Deep Sea Res. Part I. **41**, 1663–1683 (1994)
Shin, S.I.: Sensitivity of the northeast Asian summer monsoon to tropical sea surface temperatures. Geophys. Res. Lett. **38**, L22702 (2011)
Si, D., Ding, Y.: Oceanic forcings of the interdecadal variability in east Asian summer rainfall. J. Clim. **29**, 7633–7649 (2016)
Sun, S.Q., Sun, B.M.: The relationship between the anomalous winter monsoon circulation over East Asia and summer drought/flooding in the Yangtze and Huaihe River valley. Acta Meteor. Sinica. **57**, 515–522 (1995)
Twigt, D.J., De, G.E.D., Schrama, E.J.O., Gerritsen, H.: Analysis and modeling of the seasonal South China Sea temperature cycle using remote sensing. Ocean Dyn. **57**, 467–484 (2007)
Wang, L., Chen, W.: An intensity index for the east Asian winter monsoon. J. Clim. **27**, 2361–2374 (2014)
Wang, D.X., Qin, Z.H., Zhou, F.X.: Study on air-sea interaction on the interannual time-scale in the South China Sea. Acta Meteorol. Sinica. **55**, 33–42 (1997)
Wang, B., Huang, F., Wu, Z.W., Yang, J., Fu, X.H., Kikuchi, K.: Multi-scale climate variability of the South China Sea monsoon: a review. Dyn. Atmos. Oceans. **47**, 15–37 (2009)
Wilks, D.S.: Statistical Methods in the Atmospheric Sciences, p. 467. Academic Press, Cambridge (1995)
Wu, R.: Processes for the northeastward advance of the summer monsoon over the western North Pacific. J. Meteor. Soc. Japan. **80**, 67–83 (2002)
Wu, R.: Subseasonal variability during the South China Sea summer monsoon onset. Clim. Dyn. **34**, 629–642 (2010)
Wu, R., Wang, B.: Multi-stage onset of the summer monsoon over the western North Pacific. Clim. Dyn. **17**, 277–289 (2001)
Wyrtki, K., 1961: Physical oceanography of the Southeast Asian waters. Naga report, vol. 2. Scientific results of marine investigations of the South China Sea and the Gulf of Thailand 1959–1961. Scripps Institution of Oceanography, La Jolla, 195 pp.
Xie, S.P., Chang, C.H., Xie, Q., Wang, D.X.: Intraseasonal variability in the summer South China Sea: wind jet, cold filament, and recirculations. J. Geophys. Res. **112**, C10008 (2007)
Zhang, R., Delworth, T.L.: Impact of Atlantic multidecadal oscillations on India/Sahel rainfall and Atlantic hurricanes. Geophys. Res. Lett. **33**, L17712 (2006)
Zhang, R., Delworth, T.L.: Impact of the Atlantic multidecadal oscillation on North Pacific climate variability. Geophys. Res. Lett. **34**, L23708 (2007)
Zhang, L., Zhu, X., Fraedrich, K., Sielmann, F., Zhi, X.: Interdecadal variability of winter precipitation in Southeast China. Clim. Dyn. **43**, 2239–2248 (2014)
Zhu, C.W., Nakazawa, T., Li, J.P.: The 30~60 day intraseasonal oscillation over the Western North Pacific Ocean and its impacts on summer flooding in China during 1998. Geophys. Res. Lett. **30** (2003). https://doi.org/10.1029/2003GL017817